Aino Leppänen[1], Honghi Tran[2], Raili Taipale[3], Erkki Välimäki[4], and Antti Oksanen[1]

[1]Department of Chemistry and Bioengineering, Tampere University of Technology, [2]Department of Chemical Engineering and Applied Chemistry, University of Toronto, [3]VTT Technical Research Centre of Finland, [4]Valmet Power

Numerical modeling of fine particle and deposit formation in a recovery boiler

Fuel, 129:45–53, 2014.

Abstract

In kraft pulp mills, black liquor is concentrated and burned in recovery boilers to produce steam and power and to recover pulping chemicals. Black liquor contains a large amount of alkali compounds, which form ash with low melting temperatures upon combustion. This causes many problems in recovery boiler operation, including fouling of the heat transfer surfaces, plugging of the flue gas passages, reduction of the heat transfer rate, and corrosion of the superheater tubes. This paper presents a model for simulating fine fume particles formed as a result of condensation of alkali compound vapors in the recovery boiler. The modeling method combines CFD modeling, equilibrium chemistry, and fine particle dynamics in a way that enables simulation of a full scale three-dimensional boiler environment. The model has been partially validated with measurements performed in an operating recovery boiler. The modelling results, particularly for the fume particle composition, agree well with the actual measurements.

Introduction

Recovery boilers are vitally important in the pulp making process. The boilers burn the spent pulping liquor, known as black liquor, that has been concentrated at 65 to 85% dry solids. This is done to recover the pulping chemicals and to produce steam and electricity for use in the pulp mill and the possible adjacent paper mill. In modern pulp mills, a portion of the produced electricity is sold to the power grid, making the recovery boiler an important bioenergy generator.

The average size of the recovery boiler has grown considerably in recent years. The steam temperatures and pressures have also increased. These two advancements have significantly increased the power generation capability of recovery boilers, but further efficiency improvements are difficult to achieve due to the high alkali content of the black liquor. The combustion of black liquor results in a large amount of fly ash with low melting temperatures, making the boiler susceptible to massive deposit buildup (fouling) and high temperature superheater corrosion. The main compounds in the boiler ash are Na_2SO_4, Na_2CO_3, and NaCl, and the corresponding potassium compounds [1, 2]. Sodium (Na) and sulfur (S) originate mostly from the cooking chemicals, whereas potassium (K) and chlorine (Cl) originate from wood [3]. The main challenge with these alkali compounds is that they tend to build-up massively on the heat transfer tube surfaces, lowering the thermal efficiency of the boiler, and in the worst case, may lead to an unexpected shutdown of the boiler [4]. For boilers that operate at high steam temperatures ($> 490°C$), alkali chlorides in deposits can induce superheater corrosion and lead to tube thinning and eventual failure.

As the flue gas passes through the heat transfer section of the boiler, it cools causing vapors of alkali compounds to condense and form submicron particles, known as fume. Condensation occurs either directly from the gas forming condensation nuclei or onto already existing particle seeds. These fine fume particles differ from carryover particles, which are much larger (> 100 μm in diameter), and consist of partially burned black liquor [5]. The transportation of carryover particles and their deposition on boiler surfaces has been investigated and modeled by several researchers,

e.g. [6, 7, 8]. The deposition of submicron-sized particles has also been modeled by Jöller et al. [9], for example. However, the modeling of formation, transportation, and deposition of fume particles in the recovery boiler has, to our knowledge, been investigated only by Jokiniemi et al. [2]. They developed a model (which they named "ABC") for simulating the alkali metal and fume behavior, including deposition. However, since the ABC model was a 1-D (one dimensional) model based on overall gas conditions, it could not account for the effects of local gas temperature and flow field. This research group later developed a computational fluid dynamics (CFD) boundary layer model that was based on a sectional method [10], and applied the model to a 2-D case covering only a small area of the boiler.

The objective of this work is to develop a CFD based submodel for alkali metal behavior and fume formation that could be applied to a full 3-D boiler case. The program Fine Particle Model (FPM) is chosen for this purpose because it models the fine particle dynamics in a Eulerian reference frame by considering the particles as log-normally distributed particle groups [11]. This makes fine particle simulations more efficient and reduces the computing time considerably. The FPM runs together with the CFD program ANSYS Fluent, which enables the concurrent simulation of mass and heat transfer [12]. In order to model the deposit build-up, user-defined functions are also used to estimate particle deposition by thermophoresis and diffusion, and by condensation of alkali vapors on heat transfer surfaces. In addition, the presented submodel simulates the chemical reactions occurring between the alkali metal compounds by assuming that the reactions reach equilibrium.

The simulation results are compared against measurements in a full-scale recovery boiler, and the modeling results agree well with the measured fine particle composition. The simulations give additional information compared to experimental methods alone. For example, the modeling results can help to explain the relative importance of different deposition mechanisms, such as thermophoresis.

Experiments

Field measurements

Field measurements were performed in a recovery boiler with a firing capacity of 3400 tonnes of dry solids a day (tds d^{-1}). During the measurements, the boiler was running almost at full load, burning black liquor with 79.3% dry solids content and producing superheated steam rated at 480°C and 84 bar. The composition of black liquor is presented in Table 1.

The boiler has four air levels: primary, lower secondary, upper secondary, and tertiary accounting for 31.9%, 31.9%, 16.7%, and 12.7% of the total inlet air, respectively. The remaining 6.8% is the air contained in diluted non-condensable gases and vent gases.

The schematic drawing of the boiler and the measurement locations in the superheater area are, respectively, shown in Figures 1a and 1b.

Flue gas temperatures were measured with a K-type thermoprobe inserted horizontally about 1 m into the boiler through measurement ports for approximately 6 minutes. In order to determine the accuracy of the thermoprobe measurements, suction pyrometer measurements were performed at two locations. Since the results obtained were similar, only results obtained with the thermoprobe were used. The average values of 2 to 3 temperature measurements are presented in Figure 4, where the values are also compared with the modeled temperature distribution.

Table 1: Composition of black liquor (dry mass basis).

Element	C	H	S	O	N	Cl	Na	K	Inert
Wt-% (B)	33.5	3.4	6.5	34.5	0.1	0.06	20.8	0.9	0.2

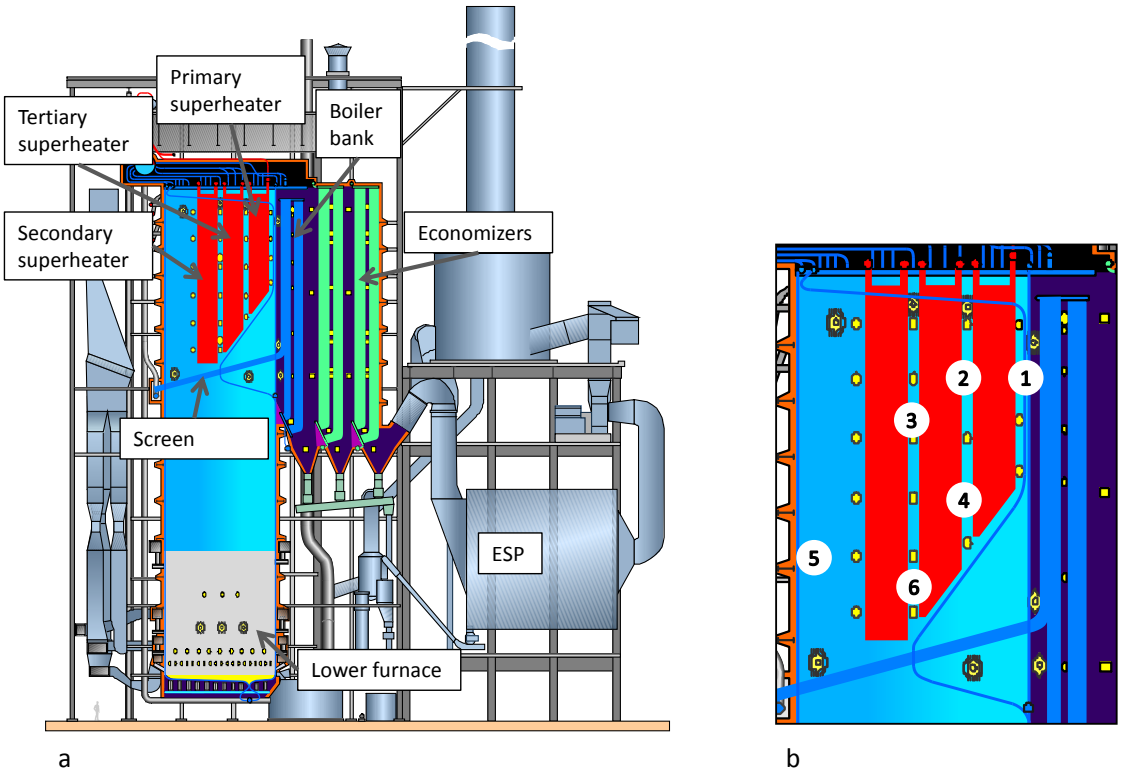

Fig. 1: a) Boiler schematic drawing and b) the measurement points in the superheater area. (Courtesy of Valmet Power.)

Fine particle measurements

Fine particles were sampled using low pressure impactors, and the samples were taken through the measurement ports shown in Figure 1. The continuous sampling time for each location ranged from 5 to 10 minutes. The measurement setup is shown in Figure 2.

Three impactors were used: an ELPI™ (Electrical Low Pressure Impactor) to monitor particle concentrations on-line, and two DLPIs (Dekati® Low Pressure Impactor) to capture two samples of particles. The distribution of particle mass in different size fractions was similar for the two DLPI samples. Cyclones with 10 µm cut-off diameters were used in front of the impactors to remove large particles from sampling. The flue gases were diluted before entering the impactors. An FTIR (Fourier Transform Infrared Spectroscopy) analyzer (Gasmet™ DX-4000 FTIR-Analyzer) was used to determine gas components and the dilution ratio (DR). The impactor measurements were conducted by VTT Technical Research Centre of Finland with a measurement technique similar to the one presented in [13]. In addition to the impactor measurements, gas chromatography (GC) and total reduced sulfur (TRS) analysis were performed, but those results are not a focus of this paper.

Impactor sampling is needed to classify the fume particle samples into several size fractions that can be analyzed later. The analysis was performed by Labtium Oy. The samples from the first impactor were analyzed for Na^+, K^+ by means of flame atomic absorption spectroscopy (FAAS), and Cl^- and SO_4^{2-} by means of ion chromatography according to SFS-EN ISO 10304-1:2009. The samples of the second impactor were analyzed for CO_3^{2-} according to SFS-EN 1484, where a TOC (Total Organic Carbon) analyzer measured the inorganic carbon, which is assumed to originate completely from carbonate. The combined mass of the analyzed ions covered approximately 90% of the sampled particle mass in each size fraction. The results of the particle analyses are presented in Section 4, where they are also compared with the modeling results. In addition to the impactor

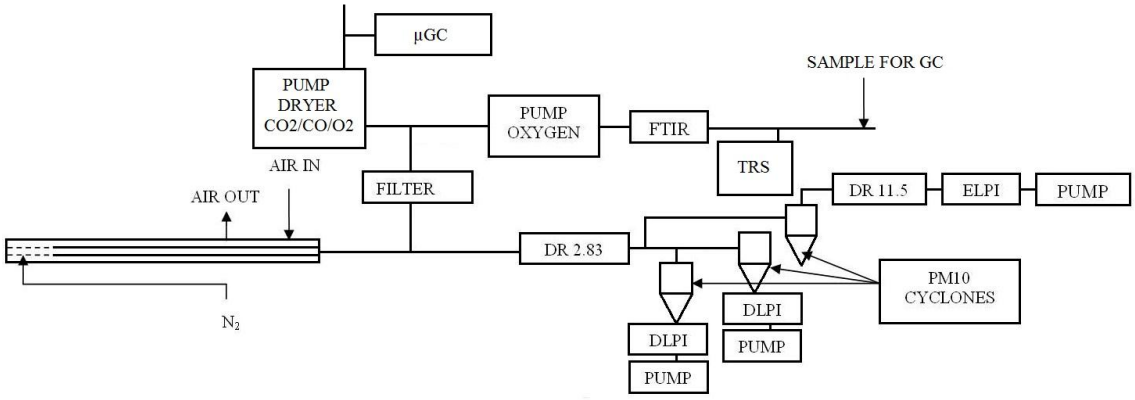

Fig. 2: Measurement equipment for fume particle measurements. (Courtesy of VTT.)

samples, the composition and amount of fly ash was measured immediately before the electrostatic precipitator (ESP).

Deposition probe measurements

Deposition probe measurements were performed in three locations, which were located above the screen (point 5 in Figure 1), after the secondary superheater (point 3), and after the tertiary superheater (point 2). At each measurement point, the probe was inserted 1 to 1.5 meters into the boiler. The probe was water-cooled to maintain its surface temperature at 450°C at point 5 and point 3, and at 480°C at point 2 to simulate the typical superheater tube surface temperatures at these locations. At all locations, the probes were kept in the boiler for 1 hour to give the fume deposit layer enough time to grow and to reach a steady-state thickness and surface temperature.

The deposit probes contained removable sampling probe rings, which were sent to Top Analytica Ltd for further composition analysis. The samples were taken from the rings by pressing a copper tape against the ring surface, coating the sampled material with platinum, and analyzing the sample with SEM-EDS (scanning electron microscopy with energy dispersive x-ray spectroscopy). For each sample, 3 to 4 different areas in the cross-section were analyzed to examine the difference in composition between the windward side deposit (facing the flue gas flow) and the leeward side deposit (on the opposite side from the flow).

Modeling methods

Computational domain

The CFD modeling in this work is performed using ANSYS Fluent [12], which solves the Reynolds-Averaged Navier-Stokes (RANS) equations and species transport equations to calculate momentum, heat, and mass transfer. The time-averaged RANS equations are used because of the large range of turbulence scales and the complex multiphysical phenomena present. A pressure-based steady-state solver is used for the calculations. Turbulence is modeled with the realizable k-epsilon model with standard wall functions, and the turbulence-chemistry interaction with the finite-rate/eddy-dissipation concept. The radiative heat transfer is modeled with the discrete ordinates model, and the pressure-velocity coupling with the SIMPLE scheme. The equations for momentum, turbulent kinetic energy, turbulent dissipation rate, energy, species mass fractions, and the user-defined scalars representing the particles are solved with second-order discretization.

The modeling domain consists of two computational grids: one for the lower furnace, and the other for the superheater section. The economizer and the ESP are not included in the model, because most particles are formed before the flue gas flow enters these colder parts of the boiler. Since the focus in this paper is on the modeling of fume formation and deposition in the superheater

Table 2: Release factors used in the model.

Element	Na	K	S	Cl
Release (%)	12	17	18	34

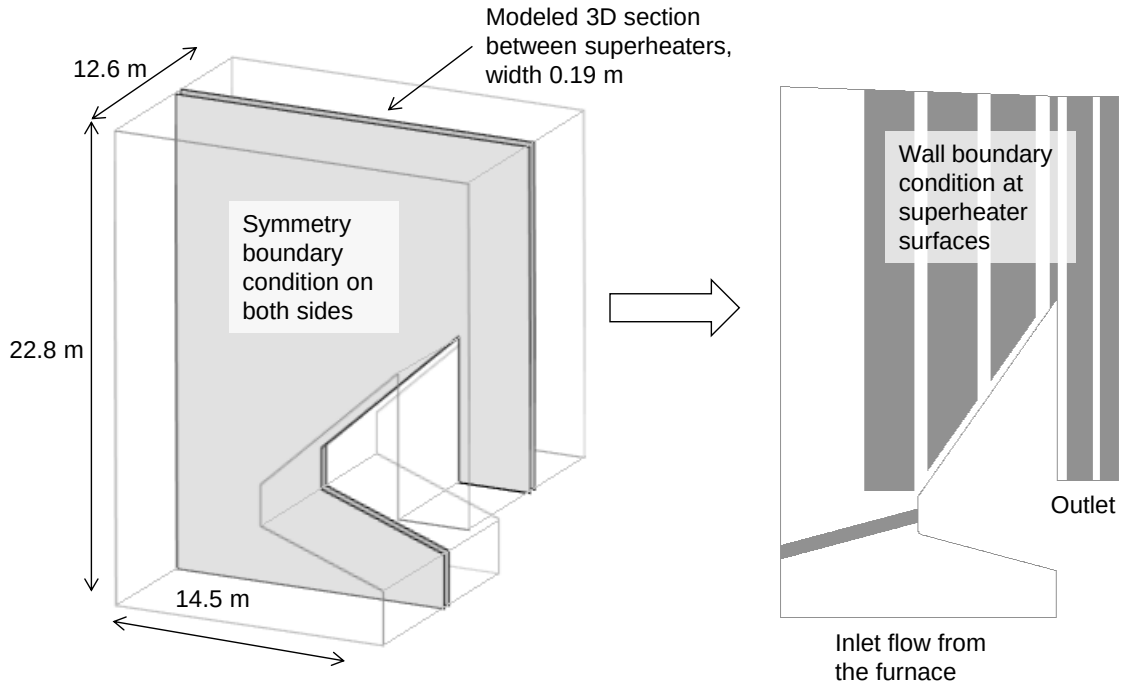

Fig. 3: Schematic of the superheater area of the boiler showing the modeled 3-D section between the superheaters, and a 2-D projection of the modeled area.

section of the boiler, the furnace modeling is only described briefly here. More details can be found in [14].

The furnace grid is 3-D, consisting of approximately 1 million structured hexahedral computational cells. It covers the injection of black liquor, the vaporization of molten alkali compounds, and the combustion of black liquor. The resulting flue gas composition and temperature are subsequentially used in the superheater grid. The combustion model used in this work is a simplified model, since our goal is not to focus on combustion reactions, but to obtain a realistic temperature field. In this work, the simplified combustion model is based on the release of the black liquor components and on the combustion of CH_4, CO, and H_2. In the present work, the composition of black liquor is taken from the measurements (Table 1). The release factors of the ash-forming elements (i.e., the fractions of the elements entering the gas stream) are based on published boiler measurement results [15, 16]. The calculated release factors are based on the difference between the amount of the elements in the as-fired black liquor and in the dust entering the ESP. The average release factors used in the model are presented in Table 2.

The superheater grid covers the area shown in Figure 3. It is also 3-D, but is denser than the furnace grid as it contains 800,000 structured hexahedral cells with grid dimensions 14.5 m x 22.8 m x 0.19 m. The grid width 0.19 m is used to cover only the area between two superheater platens. Since all cross sections of the superheater area are geometrically similar, the same grid can be extended to different sections in the superheater area by only changing the inlet boundary condition accordingly. The boundary conditions for the superheater surfaces, sides of the grid, flue gas inlet, and flue gas outlet are wall, symmetry, velocity inlet, and pressure outlet, respectively.

In addition to the original 800,000 cell superheater grid, simulations were also performed with grids consisting of 1.4 million and 2.4 million structured hexahedral cells. The results were effec-

Table 3: Flue gas temperatures for the different grids.

Grid	Point 1	Point 2	Point 3	Point 4	Point 5	Point 6
$0.8 \cdot 10^6$	703	813	894	793	954	811
$1.4 \cdot 10^6$	701	807	885	793	941	840
$2.4 \cdot 10^6$	700	806	883	795	941	838

tively the same in terms of the flue gas temperature, as can be seen in 3. For points 1 to 5, the temperature values were within 1.5% of each other. For point 6, however, the difference is larger due to recirculation of the flue gas around this point.

Fume and deposit formation was also modeled with the 1.4 million cell grid, but the results did not differ from the 800,000 cell grid in terms of the fume particle composition. This was expected because the fume formation process is governed mainly by the flue gas temperature, which was almost the same for different cell grids. Since the larger grids are computationally very demanding, the 800,000 cell grid was chosen for the final simulations.

The flue gas temperature and flow field in the superheater area are first simulated. Once the solutions have converged (approximately 2,000 iterations), these fields are used to calculate the reactions between the alkali metals, the formation of fine particles in the flue gas, and the formation of deposits on the superheater tubes. The iterations continue until the results (i.e. flue gas composition, particle composition, and particle flow rate) become constant. This stage of the calculations is time-consuming due to the easily diverging solutions for the mass fractions of NaCl and KCl, as these compounds condense rapidly near the superheater surfaces. Approximately 30,000 iterations are needed in total to reach convergence, which takes about 15 days with 8 parallel processes on an Intel® Core™ i7-3740QM processor. However, the number of iterations is expected to decrease when the simulation procedure is further developed in terms of the under-relaxation factors used, for example.

Superheater boundary conditions

In an actual boiler operation, there is always a layer of deposits on the superheater tube surface, but the thickness of this layer is not constant. The deposit layer grows due to deposition of fine fume particles and direct condensation of alkali compounds. The impaction of carryover particles also affects the deposit thickness, especially in the hotter end of the superheater area. The deposits stop growing when their surface temperature reaches the radical deformation temperature, or T_{70} (the temperature at which the deposit contains 70 wt% molten phase). Above this temperature, the fraction of molten deposit is too high for the deposit to grow [17]. Furthermore, the deposit growth is typically controlled by sootblowers which periodically blast deposits off the tube surface with high pressure steam jets. In the CFD submodel presented here, this time-dependency of the deposit thickness is not simulated. Instead, the thickness is assumed to be at a typical average value. This assumption is reasonable, since the objective of this study is to simulate how the deposit growth rate and composition are affected by boundary conditions. Simulating a time-dependent deposit thickness would require changing the computational grid in the middle of the simulations, and this is not easy computationally.

The deposit thickness determines how much heat is transferred through the deposit layer from the flue gases to the cooler metal tube, and how much the flue gas temperature decreases because of this. The tube surface temperatures are calculated based on the steam temperatures in the tubes (Table 4), and the deposit thermal conductivity is given a constant value of 1.5 W K^{-1} m^{-1}. This constant thermal conductivity gives reasonable values for the total heat transfer and is within the conductivity range given by Zbogar et al. [18]. The deposit thickness on each superheater section is assumed in order to calculate the flue gas temperature at all measurement points. The deposit thicknesses that give the best match between the measured and modeled gas temperatures are shown in Table 4, while the measured and modeled temperature values are presented in Figure 4.

Table 4: Metal surface temperatures and deposit thicknesses used as boundary conditions in the model.

Superheater	Screen	Secondary superheater	Tertiary superheater	Primary superheater	Boiler bank
Metal temperature (°C)	316	407	467	343	312
Deposit thickness (mm)	30	48	56	34	21

The deposits on the secondary and tertiary superheaters are much thicker (48 to 56 mm) than those on other tube sections (21 to 34 mm). The high average deposit thicknesses on these superheater surfaces can be justified by the presence of a large amount of sticky carryover particles in this area of the boiler.

Chemical reactions

In this model, the combustion of black liquor is assumed to completely occur in the furnace part of the boiler, while the ash-forming reactions are assumed to occur in both the furnace and superheater parts. The ash-forming elements considered are: C, Cl, H, K, N, Na, O and S. The global reactions for these elements are shown below for sodium, but the same reactions hold for potassium as well.

$$2\ \mathrm{NaCl} + \mathrm{SO_2} + \mathrm{H_2O} + \tfrac{1}{2}\mathrm{O_2} \rightarrow \mathrm{Na_2SO_4} + 2\ \mathrm{HCl} \tag{1}$$

$$2\ \mathrm{NaOH} + \mathrm{SO_2} + \tfrac{1}{2}\mathrm{O_2} \rightarrow \mathrm{Na_2SO_4} + \mathrm{H_2O} \tag{2}$$

$$2\ \mathrm{NaOH} + \mathrm{CO_2} \rightarrow \mathrm{Na_2CO_3} + \mathrm{H_2O} \tag{3}$$

The chemical reactions of the ash-forming elements are modeled as equilibrium reactions because the temperature is sufficiently high for equilibrium to be reached quickly. The local equilibria between the different inorganic compounds are calculated using the thermodynamic software FactSage [19] and its Equilib module. FactSage databases FTPulp and FTSalt are used since they contain the relevant compounds in the recovery boiler environment. The reaction equilibrium is calculated for each computational cell, and it depends both on the amount of the ash-forming elements and the flue gas temperature in that cell.

After the flow and temperature fields have been iterated to convergence and "frozen" to fixed values, the ash-forming chemical reactions are calculated together with the simulation of particle and deposit formation.

Particle formation

The most important process affecting the fume composition is condensation, which happens when gaseous compounds become supersaturated, and condense onto already existing particle nuclei. The condensing alkali metal compounds considered in our CFD submodel are: KCl, K_2CO_3, K_2SO_4, NaCl, Na_2CO_3, and Na_2SO_4.The process of particle formation through condensation has been described in more detail in [20].

The simulation of particle formation is based on the functions for aerosol dynamics available in the commercially available Fine Particle Model (FPM) [11]. The FPM is meant for simulating the formation of particles below 10 μm in diameter, which is a suitable range for the modeling of fume particles in the recovery boiler when carryover is excluded. The FPM has been used earlier mainly for the simulation of atmospheric aerosols, e.g. [21], and smaller reactors e.g. [22]. To our knowledge, there have been no other research projects where the FPM has been applied to a full-scale boiler.

In the FPM, particles are divided into distinct aerosol populations which are described by an analytical modal distribution function [23]. The log-normal distribution function is used in the FPM since it is normally chosen for aerosol populations. In contrast to the Lagrangian discrete phase model in ANSYS Fluent, the FPM models the particles in the Eulerian reference frame, and the size distributions are represented by continuous functions. This population-based treatment of particles makes it possible to efficiently simulate high particle concentrations. In the FPM calculations, the particle distribution functions are substituted into the general dynamics equation (GDE) for aerosols [24]. Through the GDE, the FPM is able to account for changes in the size distributions caused by convective transport, diffusion, sedimentation, thermophoresis, coagulation, condensation, nucleation, and source terms. For condensation, the FPM uses the expression by Barrett and Clement [25], and for coagulation, the expression by Dahneke [26].

In the presented CFD submodel, it is assumed that there are always sufficient particle nuclei available for condensation. A source of inert particle nuclei is added to the model, which allows leaving out the modeling of the unstable homogeneous nucleation. This inert nuclei assumption has also been used by Jokiniemi et al. [2] because, according to them, the resulting particle size distribution would not be significantly different if only homogeneous nucleation is simulated. The boiler measurements of Mikkanen et al. [4] also suggest that fume formation starts initially with inert nuclei, which originate from metal oxides. The initial particle source rate used in our model is 10^{14} particles $m^{-1}s^{-1}$ with a geometric diameter of 10^{-8} m, which are both approximations. The exact number concentration of the inert nuclei is not important, since coagulation will decrease the particle concentration. Furthermore, giving a small diameter for the inert nuclei ensures that their mass is negligible compared with the total mass of particles after condensation.

Deposit growth

As explained earlier in Section 3.2, this model assumes that the heat transfer surfaces are always covered with a layer of deposits. Thus, the deposition processes are calculated based on the properties of the deposit surface, not of the clean metal surface. As a consequence, the resulting deposit growth rate is given for a case where an initial deposit layer of a certain thickness has already formed on the heat transfer surface.

Thermophoresis has been experimentally shown to be the main mechanism of fume formation in the recovery boiler [27]. The thermophoretic velocity depends on the temperature gradient between a high- and a low-temperature region. The model uses the following function for the thermophoretic velocity [28]:

$$V_t = \frac{-3v\nabla T_{gs}}{4\left(1+\frac{\pi\alpha}{8}\right)T_{av}} \tag{4}$$

where v is the kinematic viscosity, ∇T_{gs} the temperature gradient between flue gas and deposit surface, T_{av} the average temperature between the flue gas and the deposit surface, and α the accommodation coefficient, which is usually about 0.9 [24]. The above equation is valid when the particle diameter $d_p \ll l$, where l is the mean free path of the gas molecules. This condition is fulfilled in the superheater region where the flue gas temperature is high. In the boiler bank area, however, the particle diameter and the mean free path of gas molecules are almost equal. Since the alternative equations for calculating thermophoretic velocity [24, 29] are much more complicated and meant for particles larger than the mean free path of gases, the Waldmann and Schmidt equation (4) is used here.

Another important deposition mechanism for fume particles is deposition by diffusion, particularly for particles below 0.1 μm in diameter [5]. The deposition velocity by diffusion is modeled with the following equation [29]:

$$V_d = \frac{0.04\bar{U}}{Re^{1/4}}\left(\frac{\rho_g D_p(T_{av})}{\eta}\right) \tag{5}$$

where $\bar{U}$ is the magnitude of gas velocity, $Re = \rho_g \bar{U} d_c / \eta$, ρ_g the density of the gas, d_c the characteristic length, η the dynamic viscosity, and $D_p(T_{av})$ the particle diffusion coefficient. In this model, $D_p(T_{av}) = D_p \cdot T_{av}/T$, where T is the standard temperature of 293 K, and $D_p = 6.94 \cdot 10^{-10}$ m^2 s^{-1}, corresponding to the diffusion coefficient of an airborne particle at standard conditions [29], when the size of the particle is 0.1 μm, corresponding roughly to the average size of the measured fume particles (see Section 4).

The third significant deposition mechanism in the recovery boiler superheater case is the direct condensation of alkali metal vapors onto the surfaces of deposits. In this case, the alkali metal vapors do not condense first onto particles, but directly onto surfaces. This condensation flux can be modeled by the following equation [30]:

$$I_v = Sh(T_g) \frac{[D_v(T_g) D_v(T_s)]^{1/2}}{d_c R_g} \left(\frac{p_v(T_g)}{T_g} - \frac{p_{v,s}(T_s)}{T_s} \right) \tag{6}$$

where $Sh(T_g) = 0.023 \cdot Re^{0.8} \cdot Sc(T_g)^{0.4}$, $Sc(T_g) = \eta / \rho_g D_v(T_g)$, $D_v(T)$ is the diffusion coefficient for gas either at the flue gas (T_g) or deposit surface (T_s) temperature, R_g the universal gas constant, $p_v(T_g)$ the partial pressure of the condensing vapor, and $p_{v,s}(T_s)$ the saturation vapor pressure of the condensing vapor at the deposit surface temperature.

Results and Discussion

Temperature has a great effect on the behavior of alkali metals, and therefore it is essential to obtain a realistic and accurate temperature field with the CFD submodel in the superheater region of the recovery boiler. The gas temperatures in the boiler were measured as described in Section 2.1. The results of the measurements (average of two or three measurements) are superimposed onto the results predicted by the CFD submodel (Figure 4). In this case, as explained in Section 3.1, the thickness of the deposit on each superheater surface was chosen so that the modeled flue gas temperatures corresponded to the measurements. The modeled value was considered acceptable if it fell within +/- 60°C of the measured value at that location.

The modeled deposit surface temperature distribution is presented in Figure 5. The deposit surface temperature is determined by the heat transfer rate from the flue gases to the superheater tube surface through the deposit layer. Mainly the flue gas temperature and the deposit thickness affect this rate. Knowing how the deposit surface temperature distributes is important, since it determines the rate of fume deposition through either direct condensation of alkali vapors or through thermophoresis and diffusion of condensed fume. Generally, the superheater areas with a lower deposit surface temperature will allow more fume to form. However, it is important to note that the temperatures presented in Figure 5 represent only the situation with the given boundary conditions. In reality, the deposit thicknesses and surface temperatures may fluctuate with time and location.

The comparison between the measured and modeled results for the fine particle composition is presented in Table 5. The measurement results are shown for three different locations and for the particle size range from 0.6 to 1.6 μm, since the majority of the particle mass was in this size fraction. The composition of the ESP ash is also shown in the table so that it can be compared with the modeled composition of the fly ash after the boiler bank (bb). The comparison is possible because all condensation should occur before the boiler bank, and the ash particle composition should be relatively constant from the boiler bank onward.

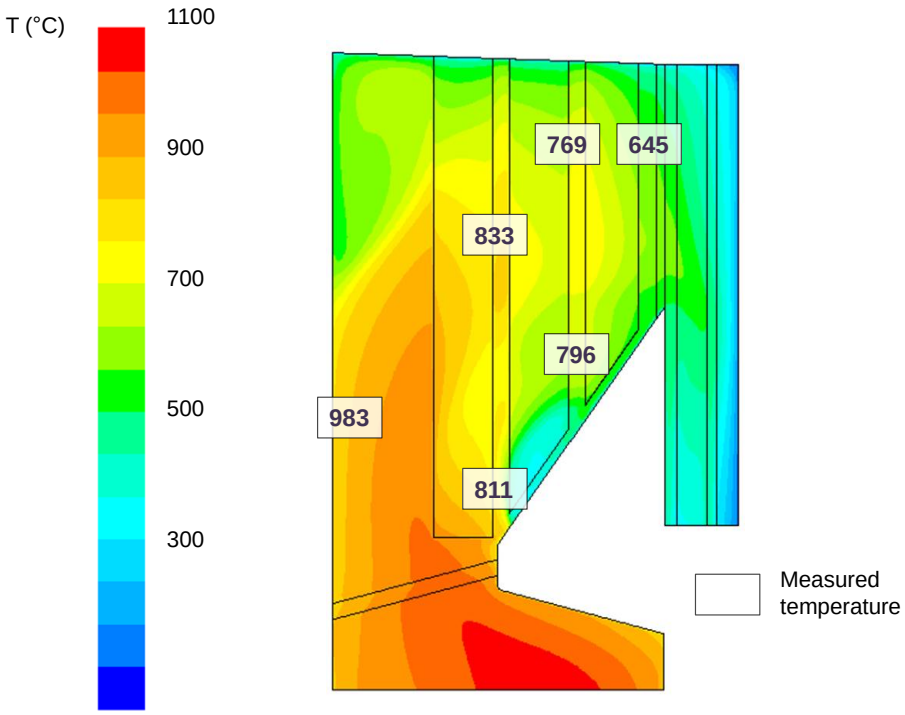

Fig. 4: Cross section of a 3D-simulation for the flue gas temperature distribution predicted by the CFD model and actual gas temperatures measured using thermoprobes.

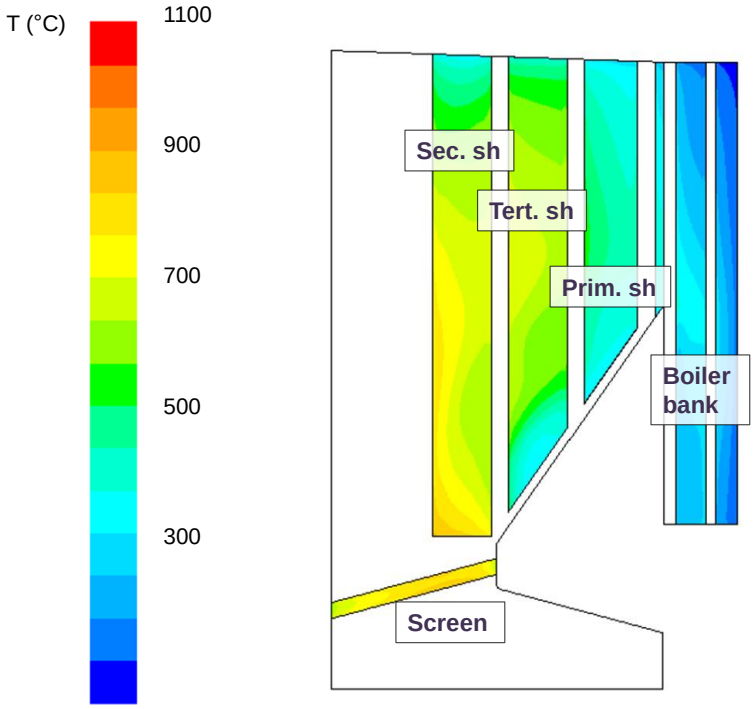

Fig. 5: Temperature distribution on the outer surface of the superheater deposits.

Table 5: Composition in wt% of the modeled and measured fine fume particles. The measurement points are shown in Figure 1b.

Grid	Point 5		Point 3		Point 2		ESP ash/after bb	
	Meas.	Model	Meas.	Model	Meas.	Model	Meas.	Model
Na	32.0	33.6	32.8	33.4	33.5	33.5	34.0	33.5
K	2.0	2.2	2.0	2.2	2.0	2.2	1.8	2.2
CO_3	13.3	14.2	12.0	13.5	11.0	14.0	12.0	13.5
SO_4	52.3	50.0	52.8	50.7	53.0	50.1	51.7	50.4
Cl	0.5	0.1	0.4	0.1	0.4	0.2	0.3	0.3

As can be seen in Table 5, there is good agreement between the modeled and measured results for the fine particles. Most of the modeling results are within 15% of the measurement results. The modeled potassium and sodium contents in the particles are in good agreement with the measurements, respectively about 2.1 wt% and 33 wt% at each measurement point. However, there are some discrepancies in the chlorine content: the modeling shows the Cl content increasing from 0.1 to 0.3 wt%, whereas the measurements show a constant chlorine content of about 0.4 wt%. The difference is probably caused by the fact that the model takes into account that gaseous alkali chlorides still exist at the hotter superheater locations (points 2, 3, and 5) due to their high vapor pressures. On the other hand, these gaseous compounds condensed in the measurement device, despite the attempt to avoid this by strongly diluting the sampled gas. Measurement accuracy may also be another reason for the discrepancy, since the low concentration of chlorine may have made its accurate analysis difficult. The agreement between the measured ESP ash composition and the modeled fume composition after the boiler bank is relatively good even with respect to the chlorine content. This is because all alkali compounds should now be condensed into particles.

Overall, there are small differences in the carbonate and sulfate contents between the measured and modeled results. The measurement results show a lower carbonate content and a slightly larger sulfate content than the modeling results. These small differences can be attributed to the release factors used in the model (see Table 2). If the sulfur release factor or the amount of sulfur in black liquor were different, it would have an effect on fume and deposit composition. The sensitivity of the modeling results to the potassium, chlorine, and sulfur release would be a good topic for future research.

Table 6 shows both the modeled and the measured deposit composition for the first three heat exchangers: the screen, the secondary superheater, and the tertiary superheater. The modeled deposit compositions for the primary superheater and the boiler bank are also shown, but there are no measurement results available for these locations. The modeled composition represents the average composition of the fume deposit layer that forms on that superheater in the given boundary conditions, whereas the measured deposit composition was obtained by deposition probes in points 2, 3, and 5. In the measurements, the composition of the deposit on the leeward side of the probe was analyzed because it contained mostly fume particles. In comparison, the deposit on the windward side consisted mostly of carryover particles, which are not a focus of this paper.

Table 6: Modeled and measured fume deposit composition (in wt%) for the first three heat exchangers. The measurement points are shown in Figure 1b.

Grid	Point 5/Screen		Point 3/Sec. sh		Point 2/Tert. sh		Prim. sh	Bb
	Meas.	Model	Meas.	Model	Meas.	Model	Model	Model
Na	30.3	34.3	30.7	34.3	30.9	34.4	34.5	34.4
K	2.2	2.3	2.4	2.3	1.9	2.3	2.3	2.3
O	47.8	45.9	48.8	45.8	47.6	45.8	45.8	45.7
S	19.2	17.5	17.0	17.4	19.6	17.3	17.2	17.3
Cl	0.5	0.0	1.1	0.1	0.0	0.2	0.3	0.3

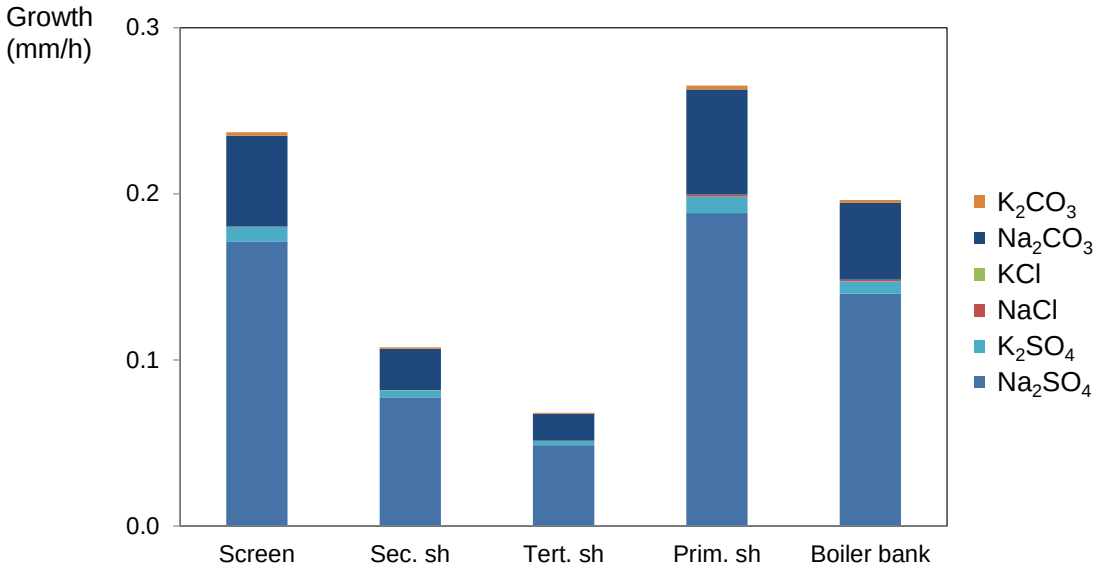

Fig. 6: Modeled average composition and growth rate of fume deposits for the superheaters.

The agreement between the modeling and the measurement values is good, because most of the modeling results fall within 15% of the measurements, similar to the fine particle modeling. This similarity is expected since the deposit composition depends on the composition of the particles in the flue gases. The differences in the modeled and measured values might be caused by the elemental release factors similar to the differences in fly ash composition. It is not possible to compare the modeling results with the measurements for the Cl content, because the measurement results are uncertain, varying from 0 to 1 wt%, since the sampling was not representative. The high variability might be caused by the low chlorine content of the black liquor, which made detection of Cl from the deposits difficult. The modeling gives the Cl content from about 0 wt% at the screen to about 0.3 wt% at the boiler bank, which is in the right direction, since the Cl content should increase as the deposit surface temperature decreases.

Figure 6 shows the modeled average deposit composition and deposit growth rate for the different superheater surfaces. The growth rate is calculated by assuming a density of 1500 kg m^{-3} for the deposit. The deposit density is difficult to approximate since it changes significantly with temperature. The value used here is based roughly on the values of Duhamel et al. [31]. Since the modeling was not time-dependent, the calculated growth rate is good only for the given boundary conditions. In reality, when the deposit thickness increases, the deposit surface temperature also increases due to the decreased rate of heat transfer. This would lower the rate of fume deposition through thermophoresis. Therefore, the modeling results should only be used to determine the relative difference in deposit growth rate between different locations in the superheater area.

Figure 6 shows that, according to the modeling results, the deposits grow more massively on the screen and on the primary superheater than on other tube surfaces. However, it is worth noting that the deposit on the screen cannot in reality grow as much as shown in the figure, because the gas temperatures near the screen (see Figure 5) are typically higher than 900°C, causing the deposit surface temperature to exceed the radical deformation (or slagging) temperature, which is around 820°C for the modeled deposit composition. This temperature is also known as T_{70}, the temperature at which the deposit contains 70 wt% molten phase. As a result, the fraction of molten deposit is so high that the deposit can no longer grow [17].

There was no measured data obtained to validate the modeled fume deposit growth rate for the superheater surfaces. However, the 1-hour deposit measurements of Mikkanen [15] gave a growth rate of 0 to 0.2 mm h^{-1} for the leeward side deposits. These measurements were conducted at a boiler similar to the one modeled in this article, and the deposition probe was positioned in a

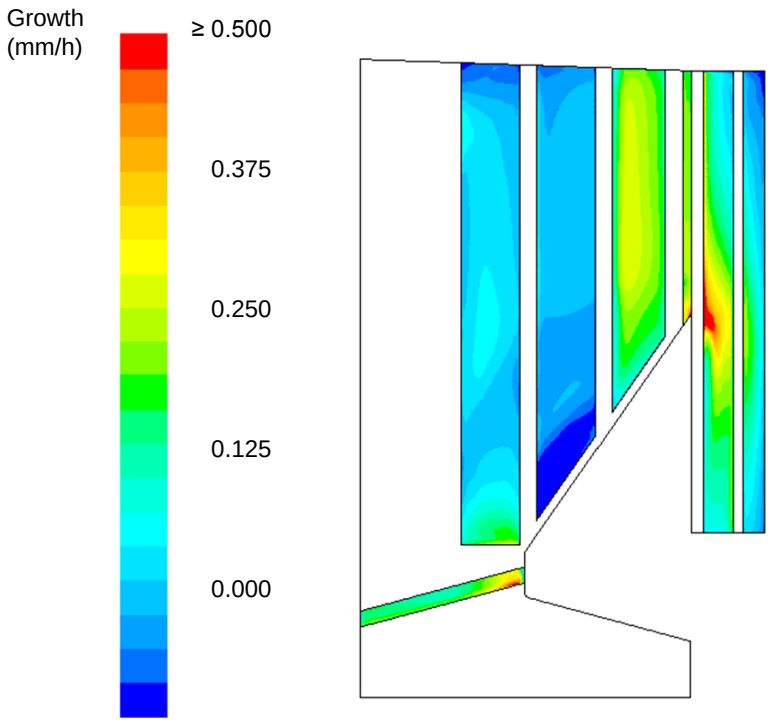

Fig. 7: Distribution of fume deposit growth rate on the superheaters.

location that corresponds roughly to the space between the secondary and tertiary superheater in the modeled boiler.

Despite the relatively good agreement with the published measurements, there is a possibility that the modeled deposit growth rate would be affected by the size of the computational grid used. Ideally, the cells near the superheater surfaces should be smaller, but this would significantly increase the grid size and the calculation time. However, the modeled deposition growth rate is similar to the value given by another fume deposition simulation by Pyykönen and Jokiniemi [10]. This simulation covered a smaller area of the boiler, and the grid was much more refined than the one used in this paper. In their work, the obtained fume deposition rate was about 7 g $m^{-2}min^{-1}$, which is, with the deposit density of 1500 kg m^{-3}, approximately 0.3 mm h^{-1}.

Figure 7 shows how the fume deposit growth rate varies between different locations in the superheater area according to the modeling results. Again, it is important to note that T_{70} is reached on the deposits on the screen and on the lower secondary superheater, and therefore the deposits there cannot grow as much as shown in the figure. However, the most significant location for fume deposit growth seems to be on the primary superheater tubes. This is because the sudden temperature drop on the superheater surfaces increases deposition by thermophoresis through an increase in the temperature gradient (see eq. 4). The primary superheater is also the area in this boiler where massive deposits are observed.

The modeling results show that most of the deposit growth is caused by thermophoresis of fine fume particles toward a colder surface, when the deposition of carryover particles is not considered. Diffusion of particles accounts only for a negligible amount of total deposition, namely less than 0.001%. The contribution of direct alkali vapor condensation is also insignificant in most areas, but it can contribute up to 0.01% of the total deposited mass at the lower primary superheater. Figure 8 shows the contribution of direct alkali vapor condensation to total deposit formation.

The small effect of direct alkali vapor condensation is due to the high number of particle nuclei available in the recovery boiler, which causes most condensation to take place on the fine particle surfaces. However, the contribution of direct alkali vapor condensation to deposition can be significant in areas where some of the alkali vapors suddenly become saturated. For example, alkali

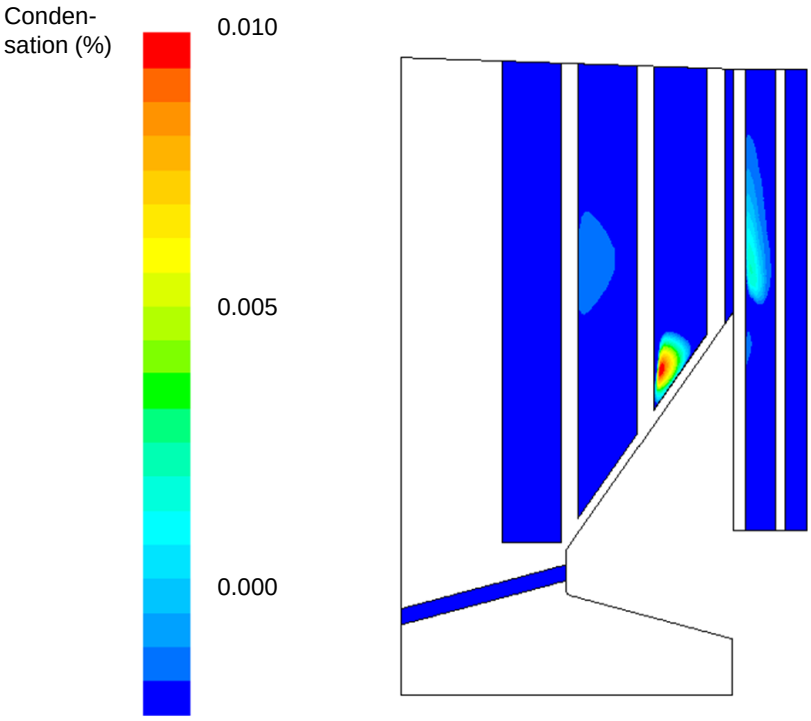

Fig. 8: Contribution of direct alkali vapor condensation on deposit growth.

sulfates and carbonates become saturated near the secondary superheater, whereas alkali chlorides tend to condense around the primary superheater. Sodium chloride becomes saturated at the primary superheater due to the sudden decrease in temperature, and the direct condensation of NaCl vapors can contribute as much as 2% of total NaCl deposition.

In addition to the growth rate, another important deposit property is the Cl content. Chlorine lowers the first melting temperature of the deposits and increases the fraction of liquid phase in them [17]. Figure 9 shows how the Cl content of the deposits changes in the superheater area.

The Cl content of the deposits increases from 0 to 0.36 wt% when the temperature decreases. This is because saturated alkali chlorides condense mainly onto particles which subsequently deposit on the tube surfaces through thermophoresis. The effect of direct alkali chloride condensation on the surface of the primary superheater does not have a noticeable effect on the Cl content due to the low level of chlorine in the black liquor. Overall, the Cl content of the fume deposits is low, but for boilers burning liquor with higher chlorine contents, the deposits might have a higher Cl content. The chlorine content of the deposits is important from the corrosion point of view, because both KCl and NaCl are known to be corrosive on steel at superheater temperatures [32].

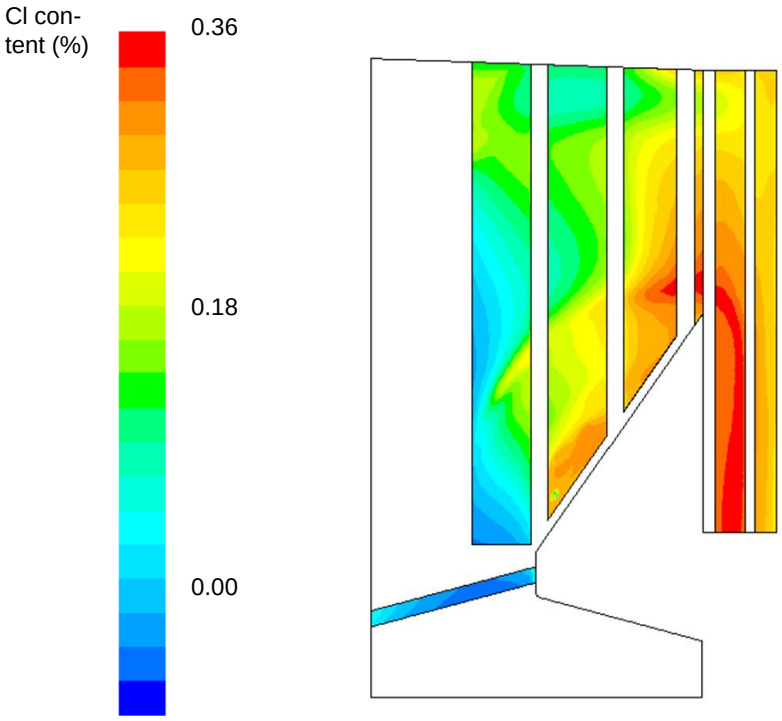

Fig. 9: Chlorine content of the fume deposits.

Conclusions

The CFD submodel presented in this paper can simulate the transformation of the alkali compounds in the kraft recovery boiler into submicron sized fume particles. The model can also simulate the deposition of these particles through thermophoresis and diffusion, and the direct condensation of the alkali compound vapors onto heat transfer surfaces. The aim of this model development is to find a way to simulate a full-scale boiler environment, which requires the use of relatively simple aerosol dynamics functions and several simplifying assumptions in order to make the model computationally feasible. The model has been partially validated with measurements in a full-scale boiler, and the results for the fume particle composition agree well with the measurements.

The modeling results indicate that the fume deposits grow fastest on the primary superheater, and indeed, the modeled boiler has been susceptible to plugging at the primary superheater. The modeling results suggest that most of the fume deposit growth at the primary superheater is due to thermophoresis of the fume particles. Carryover deposition was not considered in this work, but based on the low flue gas temperatures near the primary superheater and the low Cl content in the black liquor, the carryover particles would probably not have enough melt to stick to the surface upon impact. It can be therefore concluded that fume deposition by thermophoresis is the dominant deposition mechanism at the primary superheater in this boiler.

In this boiler, the direct condensation of alkali chloride vapors does not have much effect on the chlorine content of the deposits due to the low level of chlorine in black liquor. In general, the modeling results show that the composition of fume deposits between different superheaters does not differ significantly in terms of chlorine content, which is consistent with the simulations of Pyykönen and Jokiniemi [10]. However, the situation might be different in a boiler with higher black liquor chlorine content.

While the submodel gives results that agree well with the measurements, it has several limitations. The model is sensitive to the input parameters, such as the amount of sulfur released from black liquor, and therefore the sensitivity analysis of the model should be a topic of future study. The model sensitivity to different functions describing the aerosol dynamics should also be investi-

gated. The most important limitation lies in the fact that the simulations are not time-dependent. The results are thus only applicable to cases where the deposit thickness and surface temperature for each superheater are fixed.

Due to the steady-state nature of the model, it should be used to simulate how different changes in the boiler boundary conditions affect the behavior of the alkali compounds, fume particles, and fume deposits. For example, the model can help in understanding how the deposit growth rate and composition change when going from a clean tube surface to a situation where the deposit has grown to its maximum thickness. In the future, time-dependent modeling could be considered, but it would be computationally very demanding.

This work contributes to the existing knowledge of fume formation and deposition in recovery boilers by providing a way to simulate how these processes depend on the local conditions in the boiler, and how the fume particle and deposit composition change as a result of this.

Acknowledgements

The authors express their appreciation to Valmet Power Oy (former Metso Power Oy), Walter Ahlströmin säätiö, and the Finnish Graduate School in Computational Fluid Dynamics of the Academy of Finland for financing this project. They also gratefully acknowledge Jouni Pyykönen for proposing the principles on which the model is based, Evan Whitby for FPM support, Markus Engblom for useful discussions regarding Fluent's user-defined functions, and Anne Aikio's team for the measurement campaign. The authors also thank Carolyn Winsborough, Anna Pääkkönen, and Cyril Bajamundi for proof reading the article.

Bibliography

[1] H. N. Tran, D. W. Reeve, and D. Barham. Formation of kraft recovery boiler superheater fireside deposits. *Pulp & Paper Canada*, 84(1):36–41, 1983.

[2] J. Jokiniemi, J. Pyykönen, P. Mikkanen, and E. I. Kauppinen. Modeling fume formation and deposition in kraft recovery boilers. *TAPPI Journal*, 79(7):171–181, 1996.

[3] H. N. Tran, D. Barham, and D. W. Reeve. Chloride and potassium in the kraft chemical recovery cycle. *Pulp & Paper Canada*, 91(5):185–190, 1990.

[4] P. Mikkanen, E. I. Kauppinen, J. Pyykönen, J. K. Jokiniemi, M. Aurela, E. K. Vakkilainen, and K. Janka. Alkali salt ash formation in four finnish industrial recovery boilers. *Energy & Fuels*, 13(4):778–795, 1999.

[5] H. Tran. *Upper Furnace Deposition and Plugging*, pages 245–282. Kraft Recovery Boilers. Tappi Press, Atlanta, 1997.

[6] C. Mueller, M. Selenius, M. Theis, B.-J. Skrifvars, R. Backman, M. Hupa, and H. Tran. Deposition behaviour of molten alkali-rich fly ashes - development of a submodel for CFD applications. *Proceedings of the Combustion Institute*, 30(2):2991–2998, 2005.

[7] K. Strandström, C. Mueller, and M. Hupa. Development of an ash particle deposition model considering build-up and removal mechanisms. *Fuel processing technology*, 88(11):1053–1060, 2007.

[8] B. Li, A. Brink, and M. Hupa. CFD investigation of slagging on a super-heater tube in a kraft recovery boiler. *Fuel Processing Technology*, 105:149–153, 2013.

[9] M. Jöller, T. Brunner, and I. Obernberger. Modeling of aerosol formation during biomass combustion for various furnace and boiler types. *Fuel Processing Technology*, 88(11):1136–1147, 2007.

[10] J. Pyykönen and J. Jokiniemi. Modelling alkali chloride superheater deposition, and its implications. *Fuel Processing Technology*, 80(3):225–262, 2003.

[11] Particle Dynamics GmbH. *Fine Particle Model (FPM) for FLUENT. User's Guide*, 2003.

[12] ANSYS Inc. *ANSYS Academic Research, Release 14.5*, 2013.

[13] M. Aho, K. Paakkinen, and R. Taipale. Quality of deposits during grate combustion of corn stover and wood chip blends. *Fuel*, 104:476–487, 2013.

[14] A. Leppänen, E. Välimäki, and A. Oksanen. Modeling fine particles and alkali metal compound behavior in a kraft recovery boiler. *TAPPI Journal*, 11(7):9–14, 2012.

[15] P. Mikkanen. *Fly Ash Particle Formation in Kraft Recovery Boilers*. PhD thesis, 2000.

[16] T. Tamminen, T. Laurén, K. Janka, and M. Hupa. Dust and flue gas chemistry during rapid changes in the operation of black liquor recovery boilers: Part 2 - dust composition. *TAPPI Journal*, 1(6):25–29, 2002.

[17] H. Tran. How does a kraft recovery boiler become plugged. *TAPPI Journal*, 69(11):102–106, 1986.

[18] A. Zbogar, F. J. Frandsen, P. A. Jensen, and P. Glarborg. Heat transfer in ash deposits: A modelling tool-box. *Progress in Energy and Combustion Science*, 31(5):371–421, 2005.

[19] C. W. Bale, E. Bélisle, P. Chartrand, S. A. Decterov, G. Eriksson, K. Hack, I. H Jung, Y. B Kang, J. Melancon, A. D. Pelton, C. Robelin, and S. Petersen. Factsage thermochemical software and databases - recent developments. *Calphad*, 33(2):295–311, 2009.

[20] A. Leppänen, E. Välimäki, A. Oksanen, and H. Tran. CFD-modeling of fume formation in kraft recovery boilers. *TAPPI Journal*, 12(3):25–32, 2013.

[21] E. Herrmann, D. Brus, A. P. Hyvärinen, F. Stratmann, M. Wilck, H. Lihavainen, and M. Kulmala. A computational fluid dynamics approach to nucleation in the water-sulfuric acid system. *Journal of Physical Chemistry A*, 114(31):8033–8042, 2010.

[22] J. Han, M. Xu, H. Yao, M. Furuuchi, T. Sakano, and H. J. Kim. Simulating the transformation of heavy metals during coal or sewage sludge combustion. *Journal of Environmental Science and Health Part A*, 42(2):217–224, 2007.

[23] E. Whitby and P. McMurry. Modal aerosol dynamics modeling. *Aerosol Science and Technology*, 27:673–688, 1997.

[24] S. Friedlander. *Smoke, Dust, and Haze. Fundamentals of Aerosol Dynamics.* Oxford University Press, New York, 2nd edition, 2000.

[25] J. C. Barrett and C. F. Clement. Growth rates for liquid drops. *Journal of Aerosol Science*, 19(2):223–242, 1988.

[26] B Dahneke. Simple kinetic theory of Brownian diffusion in vapors and aerosols. *Theory of dispersed multiphase flow*, pages 97–133, 1983.

[27] J. H. Cameron and K. Goerg-Wood. Role of thermophoresis in the deposition of fume particles resulting from the combustion of high inorganic containing fuels with reference to kraft black liquor. *Fuel processing technology*, 60(1):49–68, 1999.

[28] L. Waldmann and K. H. Schmitt. Thermophoresis and diffusiophoresis of aerosols. *Aerosol science*, pages 137–162, 1966.

[29] W. Hinds. *Aerosol Technology. Properties, Behavior, and Measurement of Airborne Particles.* John-Wiley & Sons, Inc., New York, 2nd edition, 1999.

[30] J. Jokiniemi, J. Pyykönen, J. Lyyränen, P. Mikkanen, and E. Kauppinen. *Modelling ash deposition during the combustion of low grade fuels*, pages 591–615. Applications of Advanced Technology to Ash-Related Problems in Boilers. Plenum Press, New York, 1996.

[31] M. Duhamel, H. Tran, and W. J. Frederick Jr. The sintering tendency of recovery boiler precipitator dust. *TAPPI Journal*, 3(10):25–30, 2004.

[32] S. Enestam, D. Bankiewicz, J. Tuiremo, K. Mäkelä, and M. Hupa. Are NaCl and KCl equally corrosive on superheater materials of steam boilers? *Fuel*, 104:294–306, 2013.